

Article

# Effect of Hybrid Reinforcements on the Microstructure and Mechanical Properties of Ti-5Al-5Mo-5V-Fe-Cr Titanium Alloy

Shuyu Sun <sup>1,\*</sup> and Weijie Lu <sup>2</sup>

<sup>1</sup> School of Mechanical Engineering, Taizhou University, Taizhou 318000, China

<sup>2</sup> State Key Laboratory of Metal Matrix Composites, Shanghai Jiao Tong University, Shanghai 200240, China; luweijie@sjtu.edu.cn

\* Correspondence: sunshuyu@tzc.edu.cn; Tel.: +86-571-8866-1911

Received: 27 May 2017; Accepted: 27 June 2017; Published: 5 July 2017

**Abstract:** In order to investigate the different effects of trace TiB and TiC on the microstructure and the mechanical properties of Ti-5Al-5Mo-5V-1Fe-1Cr Ti alloy, two different modified Ti-5Al-5Mo-5V-1Fe-1Cr Ti alloys are fabricated via a consumable vacuum arc-remelting furnace in this work. Though the volume fractions of the reinforcements are the same in the two alloys, the molar ratio of short fibers to particles is different. The materials are subjected to thermomechanical processing and heat treatment. The effects of TiB short fibers and TiC particles on the spheroidization of  $\alpha$  phase or the refinement of  $\beta$  phase have no obvious difference during heat treatment. Subsequently, the room temperature tensile test is carried out. The area covered by the  $\sigma$ - $\epsilon$  curve of the tensile test is used to compare toughness. It is revealed that the refinement of the  $\beta$  phase and the load bearing of TiB play key roles in promoting the toughness of the alloys. TiB tends to parallel the external load during tensile tests. The distribution of TiB also changes during isothermal compression test. Owing to the competition of dynamic softening with dynamic hardening, the length direction of TiB tends to parallel to the direction of maximum shear stress during the compression, which makes TiB play the role of load bearing better.

**Keywords:** Ti-5Al-5Mo-5V-Fe-Cr titanium alloy; trace TiB and TiC; microstructure; toughness

## 1. Introduction

Ti-5Al-5Mo-5V-1Fe-1Cr titanium alloy is an important aviation structural material. The alloy composition results in the tendency of the spheroidization of  $\alpha$  phase during heat treatment. Owing to the special microstructural characteristics, the alloy presents a good combination of strength and plasticity after heat treatment [1,2]. The most common processing method for this alloy is isothermal forging. However, it may appear serious microstructural heterogeneity during isothermal compression. The experiment shows that reinforcement can solve the problem by accelerating the spheroidization of  $\alpha$  phase [2].

While continuous-SiC fiber-reinforced Ti alloys have significantly superior mechanical properties, widespread application of them has been hindered by economic factors associated with high processing costs, as well as design limitations imposed by the anisotropy of properties (exacerbated by the presence of relatively weak fiber/matrix interfaces) [3,4]. Conventional Ti alloys modified with discontinuous reinforcements, on the other hand, have been widely used in recent years [5–7]. The application of the hybrid reinforcements can achieve better results in improving mechanical properties [8–10]. However, little information is available to date concerning the different effects of short fibers and particles on Ti-5Al-5Mo-5V-Fe-Cr Ti alloy.

Two different compositions of Ti-5Al-5Mo-5V-Fe-Cr Ti alloys are fabricated in this work. One alloy is modified with only B<sub>4</sub>C, the other is modified with B<sub>4</sub>C and C. The volume fractions of the reinforcements in the two alloys are the same. Addition of B<sub>4</sub>C to Ti produces TiB and TiC during solidification by in situ chemical reaction. C to Ti also produces TiC. The reinforcements are both thermomechanically stable and essentially insoluble in Ti at all temperatures in the solid state. The in situ synthesized intermetallic reinforcements have good interfacial bonding strength due to the orientation relationships [11–13]. The advantages of the reinforced alloys also include reaction-free interfaces and ease of processing. In order to obtain good toughness, the addition of B<sub>4</sub>C or C is very small.

The solid solubility of B and C is low in Ti alloy during the solidification. Solute enrichment results in constitutional supercooling which in turn provides the driving force for nucleation and increases the nucleation rate. Furthermore, excess B and C in the solid-liquid interface also lower the growth rate of the grains [11]. The refinement of β grains and intersection of different orientated acicular α colonies within β grains retard the further growth of α [1,14].

The area covered by σ-ε curve of room temperature tensile test is used to compare toughness. The experiments show that the toughness of the modified alloys is superior to that of the alloy. The different toughening effects of trace short fibers and particles are investigated by studying the improvement of the plasticity and the strength of the modified alloys.

The β phase with BCC structure is considered with high stacking fault energy, which could accelerate dislocation climbing and crossing-slipping for dynamic softening process during isothermal compression [15]. The dynamic softening dominates the competition with the work hardening. The distribution of the reinforcements changes during isothermal compression. For comparison, the alloy specimen with the two ends not polished is used. The specimen preserves the shallow circular groove caused by turning machining on the two ends, which causes serious microstructural heterogeneity during the compression. Some α grains are elongated obviously along the direction of maximum shear stress [16]. The length direction of TiB in the B<sub>4</sub>C-modified alloy is almost the same as that of the elongated α phase in the alloy after the compression. The distribution variation of the reinforcements can promote the effective aspect ratio (length/diameter) of TiB. Therefore, the distribution variation law of the reinforcements is also the key research of this work.

## 2. Experimental Procedure

The modified alloys are fabricated by in situ synthesis method. The stoichiometric weight fractions of the raw materials including sponge Ti, B<sub>4</sub>C powder, Al, Al-Mo, Al-V, Fe, and Cr are blended uniformly, and then are compacted into pellets by forging press. The pellets are melted in a consumable vacuum arc-remelting furnace (Model VCF-10, Shanghai, China). Small addition of B<sub>4</sub>C to Ti produces TiB and TiC during solidification by chemical reaction [12]:



The molar ratio of TiB to TiC is 4:1. In addition to B<sub>4</sub>C, small addition of C powder is added in the other modified alloy. The molar ratio of TiB to TiC is 1:1. C to Ti produces TiC by chemical reaction [12]:



The volume fractions of the reinforcements in the two alloys are the same. The weight fractions of the reinforcements are shown in Table 1.

The as-cast ingots are forged at 1150 °C and are rolled at 840 °C into rods with a diameter of 15 mm. Then the rod is subjected to heat treatment. In order to control the overgrowth of grains and obtain good mechanical properties, the triplex heat treatment is employed with the following process: 830 °C/1.5 h + furnace cooling, 750 °C/1.5 h + air cooling, 600 °C/4 h + air cooling.

Ti-5Al-5Mo-5V-1Fe-1Cr Ti alloy is also prepared with the same method. The ingot of the alloy is subjected to the same thermomechanical processing and heat treatment as the modified alloys.

**Table 1.** Program materials and weight fractions of reinforcements.

Sample	B <sub>4</sub> C/wt %	C/wt %	TiB/wt %	TiC/wt %	TiB/TiC Molar Ratio
Alloy A	0.1	0	0.4	0.1	4:1
Alloy B	0.06	0.04	0.27	0.27	1:1

The specimens for the tensile test and the isothermal compression test are machined from the heat-treated rods.

For tensile testing, 30 mm gage length cylindrical specimens (6 mm wide) is used. Tensile tests are performed in a servohydraulic testing machine (Model YF28A-315/200, Shanghai, China) with a strain rate of  $0.001 \text{ s}^{-1}$ . An extensometer is mounted on the specimens to measure the tensile strains.

The compression specimens are 8 mm in diameter and 12 mm in height. The two ends of the alloy compression specimen are not polished. The isothermal compression tests are performed on a Gleeble simulator (Model GLEEBLE 3500, Shanghai, China). The compression condition is  $840 \text{ }^\circ\text{C}/0.01 \text{ s}^{-1}/60\%$  (temperature/strain rate/deformation reduction). The specimens are water quenched at room temperature immediately after the compression and then are axially sectioned.

Microstructure observations by optical microscope (OM, Model CM12, Shanghai, China), scanning electron microscope (SEM, Model JSM-6460, Shanghai, China) are conducted after the specimens are polished and etched. Moreover, transmission electron microscope (TEM, Model JZM-100CX, Shanghai, China) is also used to observe the microstructure of the specimens.

### 3. Results and Discussion

#### 3.1. Microstructure of the Materials after Heat Treatment

Figure 1a shows the microstructure of alloy A after thermomechanical processing. The reinforcements can accelerate the recrystallization of  $\beta$  grains by providing nucleation sites and accelerating diffusion. However, the microstructure is still very heterogeneous due to the segregation of the alloying elements.

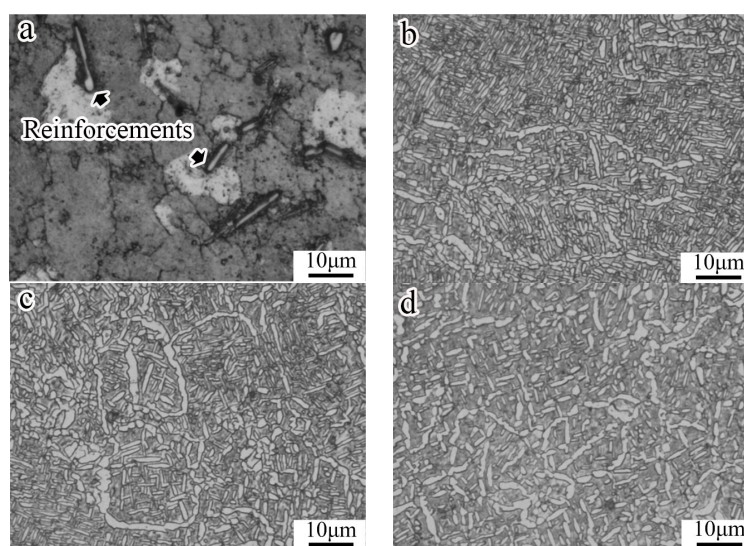


**Figure 1.** Optical microscope (OM) images of (a) alloy A after thermomechanical processing; (b) unmodified alloy after heat treatment; (c) alloy A after heat treatment; and (d) alloy B after heat treatment.

In order to measure the average grain size, the other heat treatment is used with the following process: 910 °C/1.5 h + furnace cooling, 750 °C/1.5 h + air cooling, 600 °C/4 h + air cooling. 910 °C is higher than the phase transformation temperature. Therefore, it shows the characteristics of the Widmannstatten structure in the alloys after the heat treatment [1]. The average grain size of  $\beta$  in alloy A is decreased by about 56%, and in alloy B it is decreased by about 59%. This is mainly ascribed to the Zener dragging force exerted by the reinforcements [2]. The length scales of the reinforcements are nearly the same since the additions of  $B_4C$  and C are very small. TiB has an average length of 7.9  $\mu m$  after heat treatment, while TiC 2.6  $\mu m$ . The size of TiC ranges from less than 200 nm to more than 4  $\mu m$ . A broad size distribution of particles gives rise to a larger Zener dragging force than a narrow size distribution of particles [17]. Moreover, the segregation can also exert a pinning effect on the boundary migration of  $\beta$  grain during heat treatment.

Figure 1b–d show the microstructures of the materials after heat treatment. The phase contrast is  $\alpha$  phase, white;  $\beta$  phase, black. The dislocation density in  $\alpha$  decreases significantly during the heat treatment. It appears the tendency of the spheroidization process to decrease interfacial energy due to the dispersivity of  $\alpha$  [1]. However, it is observed that trace reinforcements have no obvious effect on the spheroidization of  $\alpha$  phase during heat treatment. The decisive factor affecting the spheroidization of the  $\alpha$  phase is the first stage temperature during triplex heat treatment [18]. The increase in temperature can accelerate the boundary migration of  $\alpha$  grain, which helps to overcome the dragging force of the segregation on the boundary migration of the  $\alpha$  grain. Since the weight fraction of the reinforcements is very small, the segregation caused by the reinforcements counteracts the promoting effect of the reinforcements on the spheroidization of  $\alpha$  phase. When the temperature approaches to the phase transformation temperature, the degree of the recrystallization of  $\alpha$  phase is enhanced greatly. The reinforcements may overcome their negative effect on the spheroidization of the  $\alpha$  phase by accelerating recrystallization [18].

Figure 2 shows the microstructure of the alloy after thermomechanical processing. The phase contrast is  $\alpha$  phase, black;  $\beta$  phase, white. Primary  $\alpha$  phase almost shows as rod shaped. The  $\alpha$  phase cannot be spheroidized due to insufficient recrystallization. It appears the division of  $\alpha$  grain during heat treatment [18]. It is suggested that the rod-shaped  $\alpha$  formed during thermomechanical processing should be an important source of spheroidization grain after splitting.



**Figure 2.** Transmission electron microscope (TEM) image of the alloy after thermomechanical processing.

### 3.2. Effect of Reinforcements on the Toughness of the Alloy

Figure 3 shows  $\sigma$ - $\epsilon$  curves of the alloy, alloy A, and alloy B. The results in Figure 3 are the average values of three tensile tests for each material. The yield stresses of the materials are 1195, 1232, and 1224 MPa, respectively. If the area covered by the curve is used to compare toughness, the toughness of the reinforced alloys is superior to that of the alloy (in Figure 3). The average aspect ratio of TiB is 7.1. The critical aspect ratio of TiB can be calculated by the Kelly formula, approximately [19]:

$$l_c/d = \sigma_f / (2\sigma_{ym}) \quad (3)$$

where  $l_c$  is critical length of TiB,  $d$  is radius of TiB,  $\sigma_f$  is tensile strength of TiB (3500 MPa), and  $\sigma_{ym}$  is yield stress of matrix (1195 MP). The critical aspect ratio of TiB is about 1.46, which is lower than the average aspect ratio of TiB, significantly.

The promotion of the strengths of the modified alloys is ascribed to the load bearing of TiB, the dispersion strengthening of TiC and the grain refinement strengthening [18,20–22].

TiB short fibers tend to parallel the external force during the tensile test, which promotes the load bearing effect. The load bearing of TiB extends the strengthening process of the modified alloys. Meanwhile, the load bearing of TiB and the increase of the number of the  $\beta$  grains can improve the homogeneity of the loads applied to each  $\beta$  grain. The deformation homogeneity helps to decrease the crack nucleation.

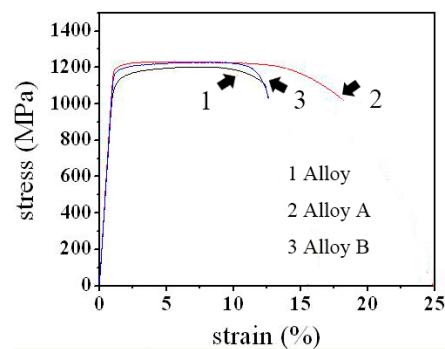


Figure 3. Stress-strain curves of the alloy, alloy A and alloy B.

Since the weight fraction of the reinforcements is very small, the negative effect of the reinforcements on the plasticity is limited. The elongation of the modified alloys is still increased during the strengthening process.

The broken TiB short fibers and TiC particles increase the propagation of crack during the necking process. Therefore, the toughening effect of the load bearing of the short fibers is mainly reflected in the strengthening process. The improvement of the reduction of area is mainly attributed to microstructural refinement during the necking process. The increase of  $\beta$  grain boundary contributes to retard crack propagation.

The tensile properties of alloy A are different from those of alloy B. The weight fraction of TiB in alloy A is higher than that in alloy B. Therefore, the load bearing of short fibers plays a more important role in alloy A. The effect of the microstructural refinement plays more important role in alloy B.

### 3.3. Microstructure of the Modified Alloy after Isothermal Compression

Figure 4 shows the microstructure of the alloy after isothermal compression. The phase contrast is  $\alpha$  phase, black;  $\beta$  phase, white. The compression specimen shows as a drum shape due to the friction between the specimen and the push rod. The macrosegregation in Figure 4a is induced by the shallow circular groove on the two ends of the specimen [16]. The metal at the center of the specimen is extruded towards the side of the specimen. Therefore, in addition to the spheroidized  $\alpha$ , some  $\alpha$  grains are elongated. Moreover, the distribution of the reinforcements in the modified alloys changes for the same reason.

The elongation of  $\alpha$  phase in Figure 4b is associated with vacancy flow. It produces a vacancy chemical potential gradient in the direction parallel to the maximum shear stress during the compression. The atomic motion is opposite to the vacancy flow. The dynamic softening dominates the competition with the dynamic hardening in  $\alpha$ . Therefore, the obstacles to the vacancy flow that caused by the dislocations is greatly reduced. The length direction of the elongated  $\alpha$  is approximated as the direction of maximum shear stress.

As shown in Figures 5 and 6, the distribution of TiB is similar to the elongated  $\alpha$  in the alloy specimen. The distribution of TiB continuously changes in order to seek the equilibrium of forces until the length direction tends to parallel to the direction of maximum shear stress during the compression.

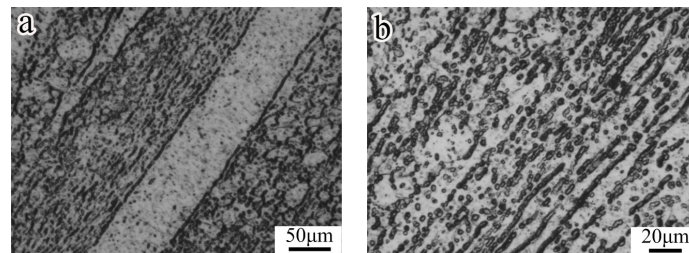


**Figure 4.** OM images of the longitudinal section of the alloy specimen after isothermal compression (a) the macrosegregation; and (b) the spheroidized and the elongated  $\alpha$ .

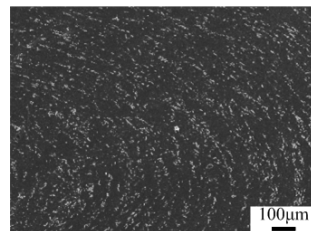


**Figure 5.** Scanning electron microscope (SEM) image of the distribution of the reinforcements in alloy A after isothermal compression.

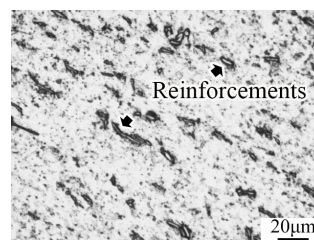


**Figure 6.** OM image of the distribution of the reinforcements in alloy A after isothermal compression.

Figure 7 shows TEM images of TiB and TiC in alloy A after isothermal compression. There also exists the competition of dynamic softening with dynamic hardening in  $\beta$  phase. As shown in Figure 7a, the end of TiB induces relatively large lattice distortion. The lattice distortion is nearly the largest when the length direction approximately parallels to the direction of maximum shear stress. Thus, the dynamic hardening gets the advantage in the competition at the ends of TiB. This plays a pinning effect on the distribution variation of TiB.

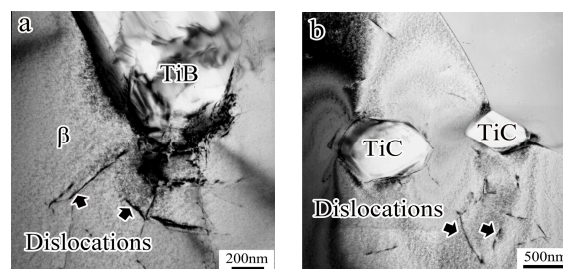


**Figure 7.** TEM images of the reinforcements in alloy A after isothermal compression (a) TiB (b) TiC.

The distribution variation of the reinforcements increases the effective aspect ratio of TiB, which allow TiB short fibers to play the role of load bearing better.

#### 4. Conclusions

- (1) The load bearing of TiB extends the strengthening process of the modified alloys. Moreover, the load bearing of TiB and the increase of the number of  $\beta$  grains can improve deformation homogeneity of the modified alloys, which decreases the crack nucleation. Therefore, the reinforcements increase the plasticity of the modified alloys. The toughening effect of the load bearing of TiB is mainly reflected in the strengthening process. The improvement of the toughness of the modified alloys is mainly attributed to the microstructural refinement during the necking process.
- (2) The distribution of TiB constantly changes in order to seek the equilibrium of forces until the length direction tends to parallel to the direction of maximum shear stress during isothermal compression. Moreover, the lattice distortion is nearly the largest when the length direction of TiB approximately parallels to the direction of maximum shear stress. This plays a pinning effect on the distribution variation of TiB. Therefore, the length direction of TiB tends to parallel the direction of maximum shear stress during the compression, which can promote the effective aspect ratio of TiB.

**Acknowledgments:** We would like to acknowledge the financial support provided by Foundation of Zhejiang Educational Committee (grant No. Y201533396).

**Author Contributions:** Shuyu Sun and Weijie Lu designed and conducted the experiments. Shuyu Sun analysed the results.

**Conflicts of Interest:** The authors declare no conflict of interesting, and the founding sponsor has no role in the design of the study; in the collection; analyses, or interpretation of data; in the writing of the manuscript, and in the decision to publish the results.

#### References

1. Sun, S.-Y.; Lv, W.-J. Microstructure and mechanical properties of TC18 Titanium alloy. *Rare Met. Mater. Eng.* **2016**, *45*, 1138–1141.
2. Sun, S.-Y.; Lv, W.-J. Effects of trace reinforcements on microstructure and tensile properties of in-situ synthesized TC18 Ti matrix composite. *J. Comp. Mater.* **2017**. [[CrossRef](#)]
3. Tamirisakandala, S.; Bhat, R.-B.; Miracle, D.-B.; Boddapati, S.; Bordia, R.; Vanover, R.; Vasudevan, V.-K. Effect of boron on the beta transus of Ti-6Al-4V alloy. *Scr. Mater.* **2005**, *53*, 217–222. [[CrossRef](#)]
4. Tanaka, Y.; Kagawa, Y.; Liu, Y.-F.; Masuda, C. Interface damage mechanism during high temperature fatigue test in sic fiber-reinforced Ti alloy matrix composite. *Mater. Sci. Eng. A* **2001**, *314*, 110–117. [[CrossRef](#)]
5. Ni, D.-R.; Geng, L.; Zhang, J.; Zheng, Z.-Z. Effect of B<sub>4</sub>C particle size on microstructure of in situ titanium matrix composites prepared by reactive processing of Ti-B<sub>4</sub>C system. *Scr. Mater.* **2006**, *55*, 429–432. [[CrossRef](#)]
6. Wang, B.; Huang, L.-J.; Geng, L.; Rong, X.-D. Compressive behaviors and mechanisms of TiB whiskers reinforced high temperature Ti60 alloy matrix composites. *Mater. Sci. Eng. A* **2015**, *648*, 443–451. [[CrossRef](#)]
7. Qi, J.-Q.; Chang, Y.; He, Y.-Z.; Sui, Y.-W.; Wei, F.-X.; Meng, Q.-K.; Wei, Z.-J. Effect of Zr, Mo and TiC on microstructure and high-temperature tensile strength of cast titanium matrix composites. *Mater. Des.* **2016**, *99*, 421–426. [[CrossRef](#)]
8. Zhang, C.; Li, X.; Zhang, S.; Chai, L.; Chen, Z.; Kong, F.; Chen, Y. Effects of direct rolling deformation on the microstructure and tensile properties of the 2.5 vol% (TiB<sub>w</sub> + TiC<sub>p</sub>)/Ti composites. *Mater. Sci. Eng. A* **2016**, *684*, 645–651. [[CrossRef](#)]
9. Shufeng, L.-I.; Kondoh, K.; Imai, H.; Chen, B.; Jia, L.; Umeda, J. Microstructure and mechanical properties of P/M titanium matrix composites reinforced by in-situ synthesized TiC–TiB. *Mater. Sci. Eng. A* **2015**, *628*, 75–83.
10. Rahoma, H.-K.-S.; Chen, Y.-Y.; Wang, X.-P.; Xiao, S.-L. Influence of (TiC + TiB) on the microstructure and tensile properties of Ti-B20 matrix alloy. *J. Alloys Compd.* **2015**, *627*, 415–422. [[CrossRef](#)]

11. Sen, I.; Tamirisakandala, S.; Miracle, D.-B.; Ramamurty, U. Microstructural effects on the mechanical behavior of B-modified Ti-6Al-4V alloys. *Acta Mater.* **2007**, *55*, 4983–4993. [[CrossRef](#)]
12. Lu, W.; Zhang, D.; Zhang, X.; Wu, R.; Sakata, T.; Mori, H. HREM study of TiB/Ti interfaces in a TiB-TiC in situ, composite. *Scr. Mater.* **2001**, *44*, 1069–1075. [[CrossRef](#)]
13. Ozerov, M.; Klimova, M.; Vyazmin, A.; Stepanov, N.; Zharebtsov, S. Orientation relationship in a Ti/TiB metal-matrix composite. *Mater. Lett.* **2016**, *186*, 168–170. [[CrossRef](#)]
14. Lütjering, G. Influence of processing on microstructure and mechanical processing. *Mater. Sci. Eng. A* **1998**, *243*, 32–45. [[CrossRef](#)]
15. Sun, Z.-C.; Yang, H.; Han, G.-J.; Fan, X.-G. A numerical model based on internal-state-variable method for the microstructure evolution during hot-working process of TA15 titanium alloy. *Mater. Sci. Eng. A* **2010**, *527*, 3464–3471. [[CrossRef](#)]
16. Sun, S.-Y.; Lv, W.-J. Microstructure heterogeneity of TC18 Ti alloy during hot deformation. *Rare Met. Mater. Eng.* **2016**, *45*, 1545–1548.
17. Eivani, A.-R.; Valipour, S.; Ahmed, H.; Zhou, J.; Duszczuk, J. Effect of the size distribution of nanoscale dispersed particles on the zener drag Pressure. *Metall. Mater. Trans. A* **2011**, *42*, 1109–1116. [[CrossRef](#)]
18. Sun, S.-Y.; Wang, L.-Q.; Qin, J.-N.; Chen, Y.-F.; Lv, W.-J.; Zhang, D. Microstructural characteristics and mechanical properties of in situ synthesized (TiB + TiC)/TC18 composites. *Mater. Sci. Eng. A* **2011**, *530*, 602–606. [[CrossRef](#)]
19. Baxter, W.-J. The strength of metal matrix composites. *Metall. Mater. Trans. A* **1992**, *23*, 3045–3053. [[CrossRef](#)]
20. Boehlert, C.-J.; Tamirisakandala, S.; Curtin, W.-A.; Miracle, D.-B. Assessment of in situ TiB whisker tensile strength and optimization of TiB-reinforced titanium alloy design. *Scr. Mater.* **2009**, *61*, 245–248. [[CrossRef](#)]
21. Tjong, S.-C.; Ma, Z.-Y. Microstructural and mechanical characteristics of in situ metal matrix composites. *Mater. Sci. Eng. R* **2000**, *29*, 49–113. [[CrossRef](#)]
22. Soboyejo, W.-O.; Shen, W.; Srivatsan, T.-S. An investigation of fatigue crack nucleation and growth in a Ti-6Al-4V/TiB in situ composite. *Mech. Mater.* **2004**, *36*, 141–159. [[CrossRef](#)]



© 2017 by the authors. Licensee MDPI, Basel, Switzerland. This article is an open access article distributed under the terms and conditions of the Creative Commons Attribution (CC BY) license (<http://creativecommons.org/licenses/by/4.0/>).